

Scalable interference from trapped ion chains

P. Obšil¹, A. Lešundák², T. Pham², G. Araneda³, M. Čížek², O. Číp², R. Filip¹ and L. Slodička^{1*}

¹ *Department of Optics, Palacký University, 17. listopadu 12, 771 46 Olomouc, Czech Republic*

² *Institute of Scientific Instruments of the Czech Academy of Sciences, Královopolská 147, 612 64 Brno, Czech Republic*

³ *Institut für Experimentalphysik, Universität Innsbruck, Technikerstraße 25, 6020 Innsbruck, Austria*

(Dated: June 13, 2024)

The demonstration of coherence between a large number of quantum emitters is essential for the realization of many paradigmatic experiments in quantum optics. Here we present the observation of controlled interference of light scattered from crystal strings of up to 53 trapped ions. The scattered light is collected along the crystal symmetry axis, which guarantees spatial indistinguishability of photons scattered by different ions and allows for convenient scaling of the number of contributing particles. The interference phase is tuned by changing the mutual distance between the ions and the observed pattern corresponds qualitatively to a simple theoretical model considering point-like emitters. The observed interference visibility remains in the 0.34 to 0.53 range for all the measured string sizes, limited mostly by the spatially inhomogeneous laser intensity seen by the long ion strings. The presented results open the possibility for experimental investigation of a whole range of fundamental physical phenomena, including engineered directional photon emission, direct detection of quadrature squeezing of atomic resonance fluorescence, and optical generation of genuine multipartite entanglement between a large number of trapped ions.

Realizing an experimental platform suitable for coherent light scattering from a large ensemble of individual quantum emitters represents a long-standing goal of the experimental quantum optics community. Its applications reach far beyond the fundamental issues studied in experimental quantum optics [1–6]. It would allow for prompt optical generation of multi-partite entangled states [7–11], controllable design and studies of collective atomic emission [12–16], and enable the realization of a feasible alternative for enhancement of absorption and collection of light in few-atom systems [15–18]. The many application prospects have been long foreseen and have stimulated the realization of a number of ingenious experiments [19–31], where the exceptional localization of the emitters has become evident in the observable coherence of the scattered light. These experiments have been technologically approached mainly from two complementary directions: one employing the convenient scalability of number of neutral atoms confined in individual optical lattice sites [19–26] and other exploiting the natural sub-wavelength localization and individual addressability of atomic ions stored in Paul traps [27–31]. The observable coherent scattering from ordered atomic ensembles have even enabled several proof-of-principle sensing applications [24, 30–33]. However, until now there has not been an experimental demonstration of a system achieving simultaneously the necessary long-term sub-wavelength spatial localization, sufficient detection efficiency of scattered light, the essential possibility of individual emitter control, and scalability with respect to the contributing number of emitters.

Here we report on the observation of interference of laser light scattered from large strings of trapped atomic

ions towards a detector positioned along the ion-crystal symmetry axis. Importantly, the implemented detection along the symmetry axis of the linear trapping potential allows for scaling up the ion number without considerable effect on their relative fluorescence collection efficiency. The spatial coherence of the detected light is guaranteed by filtering using the single-mode optical fiber and the temporal and spectral coherence is maximized by optimization of the laser cooling and saturation parameters.

The experimental scheme presented here allows for the observation of scattered light from the controllable atomic system with a well-defined number of particles and with the fundamental possibility of individual atom addressing. Fig. 1-a) shows the experimental setup, comprising a linear Paul trap with four blade-like electrodes for spatial confinement of atomic ions and the optical axis used for driving of the atoms and detection of the emitted light. The radial direction defined as the direction perpendicular to the trap symmetry axis allows for observation of the ions on an EMCCD camera with spatial resolution of each individual ion. We use it for direct determination of the ion number, string length and overall emission intensity. In the axial trapping direction, ions are confined by application of dc voltages U_{tip} on the two cone-shaped tip electrodes. The employed tip electrodes have small apertures which are typically utilized for quasi-homogeneous excitation of the ion crystals [34, 35]. Conversely, we use these apertures for the collection of light scattered by the ion crystal. After coupling the fluorescence to a single-mode optical fiber and optimization of the collection optics parameters, the presented configuration corresponds to a robust detection scheme with several crucial properties. First, for the relatively small solid angles offered by the apertures (in the order of hundreds of μm in typical setups), the light scattered from ions aligned along the optical axis of the col-

* slodicka@optics.upol.cz

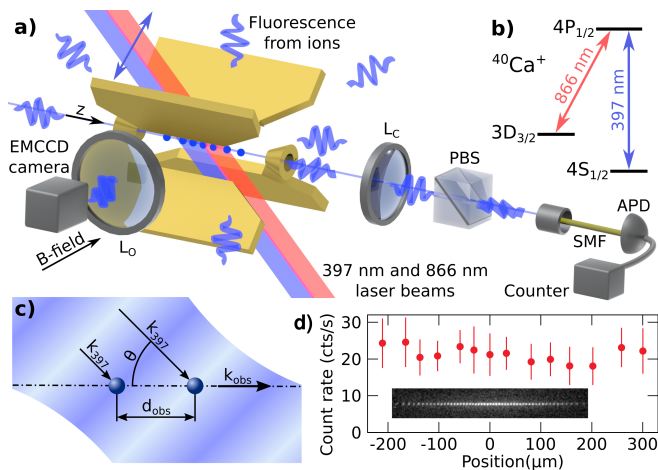


FIG. 1. a) A simplified scheme of the employed experimental setup. Ions confined in the linear Paul trap scatter the light from the exciting 397 nm laser beam and its phase interference is observed along the trap symmetry axis through a small aperture in the tip electrode. The light is collected by the coupling lens L_c and its polarization is filtered using polarization beam splitter (PBS) to maximize the portion of elastically scattered photons in the detected signal. After coupling into the single-mode fiber (SMF), the scattered light is detected by the single-photon avalanche detector (APD). The phase of the interference of scattered light is tuned by adjustment of the applied axial potential strength through voltages U_{tip} . The auxiliary observation channel used for independent estimation of the mutual ion distance and ion counting is realized along the direction of the applied magnetic field \vec{B} . b) A simplified energy level scheme of $^{40}\text{Ca}^+$ with the respective transition wavelengths. c) A scheme of the employed geometric arrangement and corresponding interfering photon paths. The measured data in d) show the dependence of the detected photon rate from single trapped ion as a function of its axial spatial position z . The inset shows the 53-ion crystal captured at the lowest employed tip voltage of $U_{\text{tip}} = 5.3$ V to illustrate the spatial extent of measured ion strings.

lection optics is detected with approximately the same efficiency as far as they lay within the Rayleigh range of the detected optical mode. Second, the axial detection configuration also allows for convenient bulk detection of the scattered light interference, because the angular gradient of the interference pattern of the collectively scattered light is expected to be the smallest close to the direction of the ion crystal axis [15]. Therefore, the presented configuration allows for maximizing the optical access with minimal effect on the observed interference visibility.

The $^{40}\text{Ca}^+$ ions are trapped with parameters chosen to achieve linear ion strings along the axial trapping direction. The radial secular frequencies are set to $f_x \approx f_y \approx 1.66$ MHz, while the axial potential is tuned in the frequency range $f_z \approx 60$ kHz–1044 kHz, corresponding to $U_{\text{tip}} = 4$ V and $U_{\text{tip}} = 900$ V, respectively. The micromotion has been carefully optimized for all employed U_{tip} settings. The ions are Doppler cooled using a

397 nm laser red-detuned from the $4S_{1/2} \leftrightarrow 4P_{1/2}$ transition, see Fig. 1-b) for the relevant energy level scheme. The population of the $3D_{3/2}$ manifold coming from the $4P_{1/2} \rightarrow 3D_{3/2}$ decay is reshuffled to the Doppler cooling transition by 866 nm laser light. The degeneracy of Zeeman states is lifted by the application of a static magnetic field with magnitude $|\vec{B}| = 6.1$ Gauss along the direction of observation on the EMCCD camera. The fluorescence in the axial trapping direction is collected using a single plano-convex lens L_c with focal length $f = 150$ mm positioned about 150 ± 2 mm from the trap center and outside of the vacuum chamber. The collected light passes a polarization beam-splitter (PBS) set for transmission of the light scattered on the σ^+ and σ^- atomic transitions in order to maximize the portion of the observed elastic scattering for the given excitation laser direction and polarization. The fluorescence is then coupled to a single-mode optical fiber (SMF) for the precise definition of its spatial mode. The photons are then detected using the single-photon avalanche photodiode (APD) with specified quantum efficiency of 77%. Together with the measured losses of optical components and estimated effective solid angle fraction of 1.3×10^{-5} , the evaluated overall detection efficiency $\eta_e = 3.7 \times 10^{-4}$ % of the light emitted from ion positioned in the center of the trap corresponds very well to the measured $\eta_m = (3.6 \pm 0.4) \times 10^{-4}$ %. The detection efficiency has been estimated by recording the 397 nm fluorescence after the excitation of spontaneous Raman transition $3D_{3/2} \rightarrow 4P_{1/2} \rightarrow 4S_{1/2}$ from an optically pre-pumped $3D_{3/2}$ manifold [36, 37]. In the presented experimental setup, this number is mainly limited by the effective solid angle fraction allowed by the apertures in the tip electrodes, however, these could be easily engineered to much larger diameters while still allowing to efficiently capture the light from tens to hundreds of trapped ions. We have estimated the width of the detection optical mode at the center of the trap by measuring the efficiency of photon detection as a function of the spatial displacement of an ion in the radial trapping direction. The Gaussian fit of the measured dependence results in detection mode waist of $w_0 = 17$ μm corresponding to a Rayleigh length of $z_R = 2.3$ mm.

The measured dependence of the detection probability of 397 nm fluorescence as a function of the axial position of a single trapped Ca^+ ion is shown in Fig. 1-d). It demonstrates the near-constant collection efficiency within the measurement uncertainties given by the shot noise and by the repeatability of the laser excitation parameters setting and within the total axial spatial position range of more than 500 μm . The error bars are estimated statistically from five consecutively measured samples for each data point. We note that the largest crystal employed in our measurements corresponding to 53 ions has estimated spatial length of 367 μm at its stretched setting corresponding to $U_{\text{tip}} = 5.3$ V. To further confirm the equality of contribution from different ions to detected light field, we have precisely measured the scaling of the detected photon rate in the pulsed generation regime for

19, 39 and 64 ions in close analogy with measurements presented in [36, 37]. We have observed linear dependence of the overall detected count rate for up to 64 ions and largest crystal length of about $340 \mu\text{m}$. These measurements clearly show the unprecedented uniformity of the fluorescence coupling efficiency into the single-mode optical fiber from long ion strings in the presented setup. Similar close-to-linear scaling is expected for even longer ion strings provided that they would be still well within the Rayleigh range of the observation light mode.

We start the observations of phase interference by looking at the simplest case of light scattering from two trapped ions. The two-ion configuration can give us important information about the relative contributions of particular decoherence mechanisms in our setup and estimation of the expectable limit on the visibility for larger numbers of ions. As can be seen in the schematic drawing in Fig. 1-c), the particular two-ion interference path arrangement closely resembles a classical Michelson interferometer. The 397 nm laser light propagating with an angle $\theta \sim 45^\circ$ with respect to the ion crystal axis can be, with a small probability, reflected off the two ions. The relative distance between two ions in the observation direction d_{obs} projected on the excitation laser beam direction gives $d_{\text{exc}} = d_{\text{obs}} \cos \theta$, which results in the overall relative phase difference $\delta\varphi = d_{\text{obs}}(1 - \cos \theta)\omega/c$, where ω is the angular frequency of the scattered light. The distance d_{obs} can be tuned by the controlling the voltage U_{tip} and its setting can be compared with the theoretically expected values [1] by independent measurement of d_{obs} on the EMCCD camera.

The data in Fig. 2-a) show measured count rates of photons scattered from two-ion crystal with 20 s overall integration time. The error bars were evaluated statistically from 5 s long data samples. The observed oscillation behavior can be reproduced by simple calculation of the observed total light intensity dependence on the relative phase $I_{\text{tot}} = 2I_1(1 + |g^{(1)}(\tau)| \cos \delta\varphi)$ shown as a solid blue curve. Here I_1 is the average light intensity from a single ion in the absence of the second ion and the $g^{(1)}(\tau)$ is the degree of first-order coherence. $|g^{(1)}(\tau)|$ in Fig. 2-a) has been scaled to find the best fit to the measured data, which is then used for estimation of the raw interference visibility $V = (I_{\text{tot}}^{\text{max}} - I_{\text{tot}}^{\text{min}})/(I_{\text{tot}}^{\text{max}} + I_{\text{tot}}^{\text{min}}) = |g^{(1)}(\tau)| = 19\%$. Here $I_{\text{tot}}^{\text{max}}$ and $I_{\text{tot}}^{\text{min}}$ are the maximum and minimum count rates from the fitted interference pattern, respectively. The estimated visibility after subtraction of spurious background counts of 9.3 ± 1.2 counts/s is $V = 34\%$, which is comparable to other observations of the phase interference with trapped ions after Doppler cooling [29–31]. It is apparent, that the observed background counts, in our case almost solely caused by detector dark counts, can contribute considerably to the detected count rate in the few-ion case for the given small collection efficiency. The phase factor $\delta\varphi$ in the presented fits has been set by independent estimation of the two-ion distance d_{obs} from calibrated axial trap frequencies f_z corresponding to axial tip voltages U_{tip} .

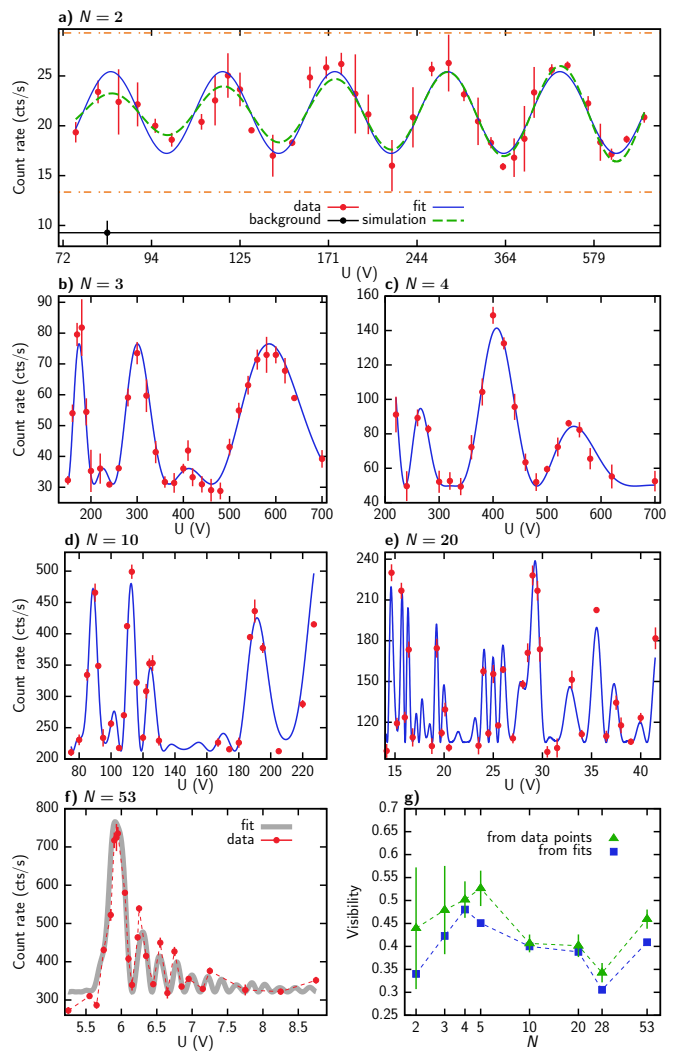


FIG. 2. Results of the measurements of phase interference of light scattered from ion crystals containing from 2 to 53 ions. The red points correspond to the measured count rates and blue solid lines show the theoretical model based on the numerical calculation of the mean relative ion positions for the given axial voltages U_{tip} , with amplitude and offset fitted to the data. All error bars correspond to statistically evaluated single standard deviation. Fig. a) shows the interference measured with 2 ions together with the full theoretical simulation taking into account the main known decoherence mechanisms (green dashed line). The measured background counts (black data point) are same for all axial voltage settings. Fig. b)-e) show samples of the interference patterns from 3 to 20 ions, respectively. Note that for more than 3 ions the mutual ion spacing is not uniform, so the expected interference patterns are not those of a regular grid. The data in f) correspond to observations of interference with $n = 53$ ions, where the Gaussian spatial beam intensity profile had to be taken into an account in order to fit the observed interference pattern plausibly (gray line). The measured visibility scaling with the ion number n estimated from the extremal data points and from fits is plotted in g).

The angle θ between the excitation and observation directions $\theta = 45.19 \pm 0.04^\circ$ has been found by the best fit to the measured data, in good agreement with the independently measured value of $\theta_m = 45.24 \pm 0.06^\circ$.

The well known substantial contributions to the interference visibility decrease in experiments concerned with scattering of the coherent light from a trapped ion crystal correspond to inelastic light scattering and motional dephasing [29–31, 39]. For the presented two-ion case, the ratio of elastic to inelastic scattering has been found by the independent estimation of the laser excitation parameters using dark-resonance spectroscopy and a corresponding theoretical model based on eight-level optical Bloch equations. The effective saturation parameter of the 397 nm laser on the $4S_{1/2} \leftrightarrow 4P_{1/2}$ transition has been found to be $s_{397} = 0.51$, which, according to numerical simulations, accounts for the reduction of the observable visibility by a factor of 0.66. The jitter in the relative position of the two ions due to their secular motion can be taken into account by including the Gaussian position uncertainties corresponding to the thermal population of the radial zig-zag and axial stretch modes with motional frequencies and mean phonon numbers measured separately for the same trapping and laser-cooling conditions [30, 31]. The resulting simulation taking into account both effects is shown as the green dashed line in Fig. 2-a). It reproduces well the measured interference pattern without any free fitting parameter. This again underlines the high degree of control of both motional and internal excitation parameters in the ion-trapping platforms represented here by a relatively conventional ion-trapping arrangement. The observed visibility decrease for the lower axial confinements is explained by the corresponding increase in the relative position uncertainty.

Figs. 2-b) to e) show measured interference patterns for 3, 4, 10, and 20 ions, respectively. Since the trapping potential produced by the Paul trap is approximately harmonic, the separation between ions for more than 3 ions is not uniform, and in general it has to be calculated numerically [1]. The observed interference patterns prove the ability of these large ion strings to scatter light in a partially phase-coherent way. The blue curves in Figs. 2-b) to e) correspond to the calculation of the observed interference, which assumes equal coherent contributions from all ions with the phase factor calculated according to the numerically estimated mean ion positions given by U_{tip} [1]. The visibilities of the calculated interference fringes are scaled to fit the experimentally observed signal, which gives us an estimate of the local interference visibility V , in analogy with the two-ion case. This simplified calculations are in very good agreement with the observed interference pattern, which suggests that the spatial distribution of ions in the crystal correspond exactly to the ideal positions given solely by the axial trapping potential and the mutual Coulomb repulsion. In addition, this points to the near-equality of the coherent contribution to the detected signal for all individual ions

present in the crystal, see Supplemental Material, Sec. A. The exactly measured spurious background counts corresponding mostly to detector dark counts has been subtracted to enhance and unify the presentation, however, it presents a much less significant limit for these large ion strings compared to the two-ion case due to the substantially higher measured count rates. The measured data in Fig. 2-f) show the observed interference pattern when scanning the tip voltage for the string containing 53 ions. In order to plausibly describe the observed data, we include the effective width of the Gaussian intensity profile of the excitation 397 nm laser beam projected on the axial direction $w_{\text{eff}} = 115 \mu\text{m}$, see Supplementary Materials A for the description of simulations. The excitation beam width presents technical limit of our particular optical setup, which could be relatively easily overcome by the employment of the elliptical laser beams. However, we believe, that the measured range of ion numbers suffices for the intended demonstration of the scalability and preservation of the optical coherence with increased ion number in the presented experimental platform. To support our conclusions about the source of modulation of the detected count rate in the presented data, we have also checked the total intensity of the ion string on the EMCCD camera, which has always remained constant within the measured ranges of U_{tip} . The number of ions in the crystal has been also precisely counted for each crystal realization resulting in zero uncertainty estimated from the counting statistics.

The observed scaling of the interference visibilities is summarized in Fig. 2-g). The visibilities are estimated from extremal data points in the locally observed interference pattern (green triangles) and from the fitted numerical model (blue squares). Remarkably, the visibility values clearly remain within the range 0.34 to 0.53 for all measured ion numbers. The deviations between the observed visibility values within this range are most likely caused by the diversity of trapping and laser-cooling parameters. In particular, since we were not able to find satisfactory global settings working for all ions, we have searched for the optimal cooling and trapping conditions with respect to achieving maximal visibility values for each given ion number. Due to the large parameter space, this in principle allows for observable variations in the measured visibilities. In addition to the interference visibility, other conventional characteristics of phase interference patterns, especially the spatial phase resolution and the overall detected count rate scaling with the number of participating ions can further facilitate the applicability of the observed results in quantum topics experiments. This analysis can be found in the Supplemental Material C.

The presented observations of the coherent scattering from trapped-ion crystals containing up to 53 ions correspond to the first unambiguous proof of collective coherent interaction of light with such large samples of individual quantum emitters. Similar observations have so far been limited to the domain of single or few scat-

terers limited mostly by the design of the interference setup geometry [23, 27, 29–31]. The observed interference patterns have the potential to trigger substantial experimental progress in many fundamental and applied research directions [1–18] which require collective coherent enhancement from many scatterers and, at the same time, high control over their external and internal degrees of freedom and the fundamental possibility of their addressing. For example, we anticipate the direct extension of the presented results to optical creation of large atomic Dicke states, which can be transformed using the addressed ion excitations to a large class of multi-qubit entangled states with broad prospects of applications. The addressed spin flips or phase shifts on individual ions prepared in a collective state of internal atomic lev-

els could be utilized for efficient control of the direction and phase of the collective optical emission, presenting a viable alternative to a free-space or cavity-mediated ion-photon coupling schemes [32]. This would allow for harvesting the unique possibilities of high fidelity internal state preparation in trapped ion platforms for deterministic control and increased efficiency of the coupling between light and atoms in free space.

We acknowledge the kind technological support from the group of Rainer Blatt including the contribution of Yves Colombe and Kirill Lakhmanskii to the construction of the employed linear Paul trap. We thank D. H. Higginbottom for useful comments on the manuscript. This work has been supported by the grant No. GB14-36681G of the Czech Science Foundation and Palacký University IGA-PrF-2017-008.

-
- [1] R. H. Lehberg, *Phys. Rev. A* **2**, 883 (1970).
- [2] D. Porras and J. I. Cirac, *Phys. Rev. A* **78**, 053816 (2008).
- [3] C. Skornia, J. von Zanthier, G. S. Agarwal, E. Werner, and H. Walther, *Phys. Rev. A* **64**, 063801 (2001).
- [4] R. T. Sutherland and F. Robicheaux, *Phys. Rev. A* **94**, 013847 (2016).
- [5] M. O. Scully, *Phys. Rev. Lett.* **102**, 143601 (2009).
- [6] T. Kauten, R. Keil, T. Kaufmann, B. Pressl, Č. Brukner, and G. Weihs, *New J. Phys.* **19**, 033017 (2017).
- [7] C. Cabrillo, J. I. Cirac, P. Garcia-Fernandez, and P. Zoller, *Phys. Rev. A* **59**, 1025 (1999).
- [8] L. Slodička, G. Hétet, N. Röck, P. Schindler, M. Hennrich, and R. Blatt, *Phys. Rev. Lett.* **110**, 083603 (2013).
- [9] C. Thiel, J. von Zanthier, T. Bastin, E. Solano, and G. S. Agarwal, *Phys. Rev. Lett.* **99**, 193602 (2007).
- [10] A. Maser, R. Wiegner, U. Schilling, C. Thiel, and J. von Zanthier, *Phys. Rev. A* **81**, 053842 (2010).
- [11] Z. Ficek and R. Tanaš, *Phys. Rep.* **372**, 369 (2002).
- [12] W. Vogel and D.-G. Welsch, *Phys. Rev. Lett.* **54**, 1802 (1985).
- [13] R. G. DeVoe and R. G. Brewer, *Phys. Rev. Lett.* **76**, 2049 (1996).
- [14] L. L. Jin, M. Macovei, S. Q. Gong, C. H. Keitel, and J. Evers, *Opt. Commun.* **283**, 790 (2010).
- [15] C. J. Mewton and Z. Ficek, *J. Phys. B* **40**, S181 (2007).
- [16] J. P. Clemens, L. Horvath, B. C. Sanders, and H. J. Carmichael, *Phys. Rev. A* **68**, 023809 (2003).
- [17] B. Casabone, K. Friebe, B. Brandstätter, K. Schüppert, R. Blatt, and T. E. Northup, *Phys. Rev. Lett.* **114**, 023602 (2015).
- [18] S. Oettel, R. Wiegner, G. S. Agarwal, and J. von Zanthier, *Phys. Rev. Lett.* **113**, 263606 (2014).
- [19] G. Birkel, M. Gatzke, I. H. Deutsch, S. L. Rolston, and W. D. Phillips, *Phys. Rev. Lett.* **75**, 2823 (1995).
- [20] C. Weitenberg, P. Schauf, T. Fukuhara, M. Cheneau, M. Endres, I. Bloch, and S. Kuhr, *Phys. Rev. Lett.* **106**, 215301 (2011).
- [21] M. Weidemüller, A. Görlitz, T. Esslinger, and T. W. Hänsch, *Phys. Rev. Lett.* **75**, 4583 (1995).
- [22] S. Slama, C. von Cube, B. Deh, A. Ludewig, C. Zimmermann, and P. W. Courteille, *Phys. Rev. Lett.* **94**, 193901 (2005).
- [23] A. Neuzner, M. Körber, O. Morin, S. Ritter, and G. Rempe, *Nat. Photonics* **10**, 303 (2016).
- [24] G. Raithel, G. Birkel, A. Kastberg, W. D. Phillips, and S. L. Rolston, *Phys. Rev. Lett.* **78**, 630 (1997).
- [25] A. Schilke, C. Zimmermann, P. W. Courteille, and W. Guerin, *Phys. Rev. Lett.* **106**, 223903 (2011).
- [26] H. L. Sørensen, J.-B. Béguin, K. W. Kluge, I. Iakoupov, A. S. Sørensen, J. H. Müller, E. S. Polzik, and J. Appel, *Phys. Rev. Lett.* **117**, 133604 (2016).
- [27] U. Eichmann, J. C. Bergquist, J. J. Bollinger, J. M. Gilligan, W. M. Itano, D. J. Wineland, and M. G. Raizen, *Phys. Rev. Lett.* **70**, 16 (1993).
- [28] W. M. Itano, J. C. Bergquist, J. J. Bollinger, D. J. Wineland, U. Eichmann, and M. G. Raizen, *Phys. Rev. A* **57**, 4176 (1998).
- [29] J. Eschner, C. Raab, F. Schmidt-Kaler, and R. Blatt, *Nature* **413**, 495 (2001).
- [30] S. Wolf, J. Wechs, J. von Zanthier, and F. Schmidt-Kaler, *Phys. Rev. Lett.* **116**, 18 (2016).
- [31] L. Slodička, G. Hétet, N. Röck, S. Gerber, P. Schindler, M. Kumph, M. Hennrich, and R. Blatt, *Phys. Rev. A* **85**, 043401 (2012).
- [32] G. Araneda, D. B. Higginbottom, L. Slodička, Y. Colombe, and R. Blatt, *Phys. Rev. Lett.* **120**, 193603 (2018).
- [33] M. Weidemüller, A. Görlitz, T. W. Hänsch, and A. Hemmerich, *Phys. Rev. A* **58**, 4647 (1998).
- [34] P. Schindler, D. Nigg, T. Monz, J. T. Barreiro, E. Martinez, S. X. Wang, S. Quint, M. F. Brandl, V. Nebendahl, C. F. Roos, *et al.*, *New J. Phys.* **15**, 123012 (2013).
- [35] H. Häffner, C. F. Roos, and R. Blatt, *Phys. Rep.* **469**, 155 (2008).
- [36] D. B. Higginbottom, L. Slodička, G. Araneda, L. Lachman, R. Filip, M. Hennrich, and R. Blatt, *New J. Phys.* **18**, 093038 (2016).
- [37] P. Obšil, L. Lachman, T. Pham, A. Lešundák, V. Hucl, M. Čížek, J. Hrabina, O. Číp, L. Slodička, and R. Filip, *arXiv preprint arXiv:1705.04472* (2017).
- [1] D. F. V. James, *Appl. Phys. B* **66**, 181 (1998).
- [39] T. Wong, S. M. Tan, M. J. Collett, and D. F. Walls, *Phys. Rev. A* **55**, 1288 (1997).

SUPPLEMENTAL MATERIAL: SCALABLE INTERFERENCE FROM TRAPPED ION CHAINS

A. Simulations of measured visibility patterns

The structure of the observed interference patterns presented in the main text could be precisely reconstructed by the simple simulation requiring only the knowledge of the tip voltages U_{tip} and the angle between the excitation and observation direction θ . The precise position of each ion in the trap along the axial trapping direction can be evaluated using the relative coefficients in equation (5) from ref. [S1]. The axial center-of-mass (COM) motional frequency has been found experimentally on single trapped ion and adjusted for the given particular number of ions using the same equation. The relative position of individual ions allows us to calculate the relative phase shift $\Delta\phi$ relevant for the observed interference pattern. The observed count rate is then, in the ideal case of 100% interference visibility and fully coherent light scattering process, proportional to light intensity

$$I_{\text{coh}} = \left| \sum_{j=1}^N A_j e^{i\Delta\phi_j} \right|^2, \quad (\text{S1})$$

where A_j is the amplitude of light scattered by j -th ion in the observation direction. A_j has been set to the unity value for all contributing ions from the string for all measured ion strings containing up to 20 ions. The obtained ideal interference pattern as a function of tip voltages U_{tip} has been then scaled to best fit of the measured count rate using

$$I_{\text{obs}} = I_{\text{incoh}} + \kappa \cdot I_{\text{coh}}, \quad (\text{S2})$$

where we fit parameters I_{incoh} and κ correspond to the incoherent light offset including the detected background counts and relative coherent contribution, respectively. For the simulations of the interference measurements realized on 28 and 53 ions, the amplitude of the light coherently scattered by ions at different axial spatial positions z is not constant and includes the Gaussian spatial modulation of the exciting 397 nm beam intensity,

$$A_j(z) = A_j(0) \frac{1}{\sqrt{2\pi}\sigma_z} \exp(-z^2/(\sigma_z^2)). \quad (\text{S3})$$

Here, the additional fitting parameter σ_z corresponds to the width of 397 nm laser beam intensity profile on the string axis.

The visibility estimated from the simulated interference patterns can be then expressed as

$$V = \frac{I_{\text{obs}}^{\text{max}} - I_{\text{obs}}^{\text{min}}}{I_{\text{obs}}^{\text{max}} + I_{\text{obs}}^{\text{min}}}, \quad (\text{S4})$$

where superscripts *min* and *max* refer to the minimum and maximum of the simulated interference pattern

within the measured range of tip voltages, respectively. We note, that for very low axial trapping potentials, a slight positive difference between U_{tip} values in simulation and in the experiment has been required for plausible reconstruction of the observed interference patterns. The magnitude of this deviation is several tens of mV at several volts of applied U_{tip} , which could be likely explained by the residual stray fields or patch potentials seen by the ions [S2, S3].

B. Illustration of individual coherent contributions

The ratio of the coherent to incoherent contribution of light scattered from ions is extremely important and can be inferred from the visibility shown in the Fig. 2-g) in the main part of the article. However, the evaluated visibility is a global figure of merit and it does not reflect the possible inhomogeneity of amplitude of coherent contributions from ions. An example of such situation could be caused by inhomogeneous intensity distribution of the scattered laser beam across the long ion strings. To illustrate the dependence on the coherent contribution of each individual ion of the interference signal we consider the measurement with 20 ions. In this case, the measured interference is well described by the simple model presented in Supplemental Material A, where each scatterer contributes equally.

If we consider that some of the ions scatter fully incoherently, the expected interference signal notoriously differs from the observed one. For example, if the two outermost ions are set to emit fully incoherent light, they still contribute to the overall offset count rate, but do not contribute to the shape of the observable intensity pattern. Importantly, due to the re-scaling of the offset I_{incoh} and amplitude parameter κ to obtain the best fit, this procedure is independent of the actual incoherent contribution. However, keeping the ions rather than removing them completely still allows us to simulate the more relevant case of ions being present but not contributing coherently. We note that complete removal of the ions from the string causes expectable radical shift and change of the whole interference pattern, because the relative positions of ions for given tip voltage would substantially differ. The simulation with two outermost ions switched to incoherent scaled to best fit the measured data is shown with a solid green line in Fig. S1-a). The obvious negative impact on the ability to reproduce the measured pattern is most notable in the height of constructive interference peaks. While some are enhanced, e.g., the first from the left, few other stay approximately similarly high, and some peaks are substantially suppressed, e.g., the peaks at 19 V and 29 V. The attempted best fit thus cannot anymore reproduce the data plausibly. The situation is phenomenologically similar for the case where the two innermost ions emit fully incoherent light, see Fig. S1-b). Switching of only single innermost or outermost ion to incoherent scatterer would show very similar behaviour

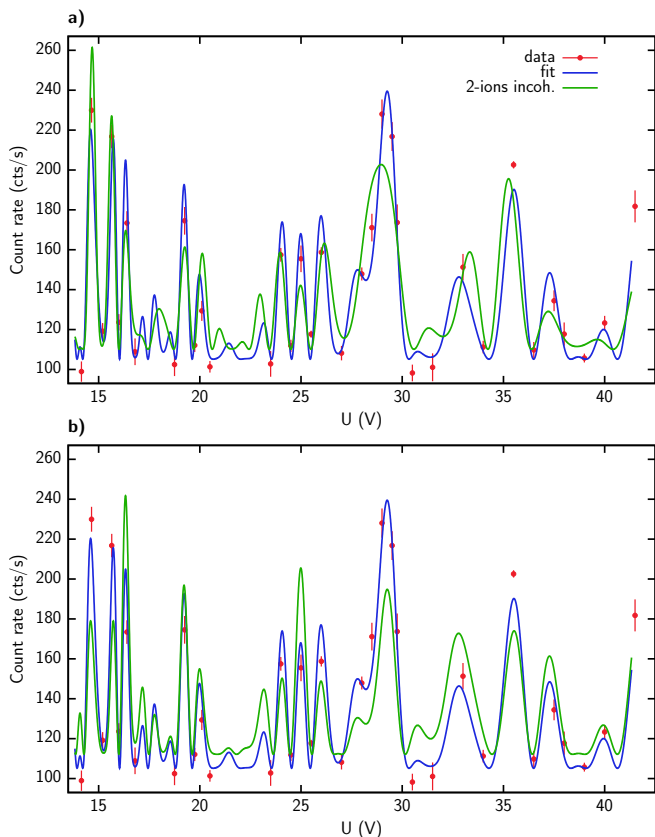


FIG. S1. Illustration of the impact of the relative change of the coherent contribution among ions in the string on the reproducibility of the measured phase interference patterns. The red points correspond to the measured data and the blue solid line is the best fit using the simulation where all 20 ions contribute with the same coherent contribution. The green solid line shows the best fit using the simulation where some of the ions were switched to fully incoherent scatterers. Graph a) illustrates the comparison of equal coherent contribution to the case where outermost two ions were switched to fully incoherent scatterers. In graph b), the comparison to simulation where the innermost two ions in the string are contributing only incoherently.

to the above mentioned cases where two ions were symmetrically switched to incoherent and it would result in half of the observed effect of two ions in the simulated interference patterns.

Perhaps the most likely situation corresponds to the case where the fraction of the coherent scattering changes continuously with the distance from the center of the ion chain which coincides with the center of the exciting laser beam. We take this into an account by implementing the Gaussian distribution of the coherent to incoherent fraction of scattering processes as a function of the distance from center of the string into the simulation. We consider two particular threshold cases, where the ions in the string center are scattering fully coherently (incoherently) and the outermost ions are scattering with

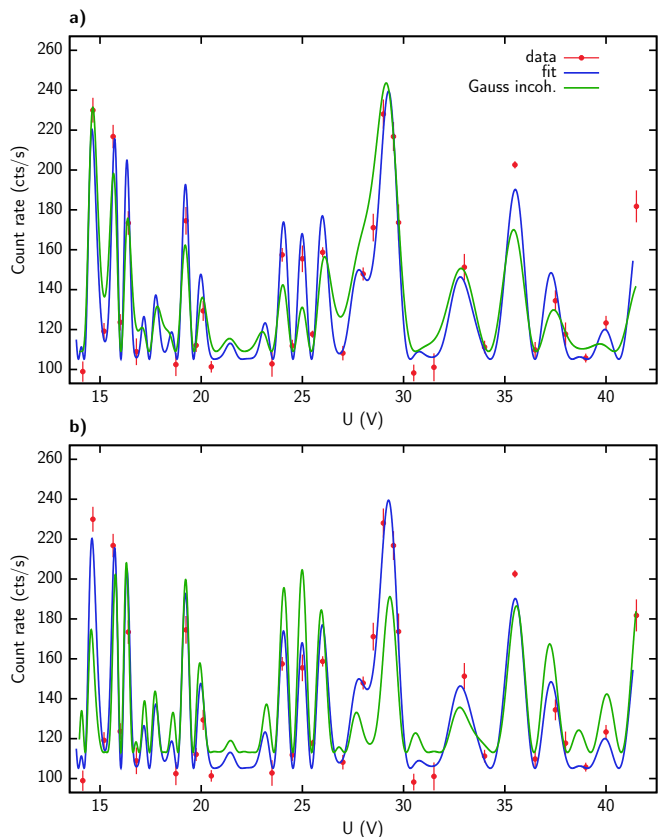


FIG. S2. Illustration of the impact of the relative change of the coherent contribution among ions in the string on the reproducibility of the measured phase interference patterns. The red points correspond to the measured data and the blue solid line is the best fit using the simulation where all 20 ions contribute with the same coherent contribution. The green solid line shows the best fit using the simulation where some of the ions were switched to partially incoherent scatterers. Graph a) illustrates the comparison of equal coherent contribution to the case of Gaussian modulation of the coherent contribution. The fully coherent scatterers are in the middle while at the each edge of the crystal the emitters scatter coherently only with the probability of $1/e$. In graph b), the coherent and incoherent parts of the gaussian modulation were switched, that corresponds to fully coherent scattering on the outermost ions in the string and coherent scattering with the the probability of $1/e$ in center of the string.

$1/e$ fraction of the coherent (incoherent) contribution, see Fig. S2-a) and b), respectively. Similarly as in the case of switching some ions to fully incoherent, these simulations lead clearly to patterns which can not plausibly reconstruct the observed data.

Note that these illustrations are not a proof of the strictly equal coherent contribution from all ions in the string. However, they show that it is unlikely that the observed interference patterns can be explained without substantial relative contribution of any ion captured within the measured ion string. In addition, they directly point on the high sensitivity of the observed interference

effect to the individual ion contributions which suggest the applicability of the presented scheme for partial or full switching of the scattered light in the given observation direction.

C. Characterization of the interference pattern scaling

To facilitate the further applicability of the observed coherent scattering and the related prospect experiments with improved axial optical access or even with different experimental platforms, we have analyzed the evolution of two important complementary characteristics of multi-slit interference experiments: the scaling of the phase resolution and the peak fringe intensity. In the context of a charged particles in a static harmonic electric potential, it is particularly interesting to compare these measures as they have been mostly studied in the case of equally spaced reflectors, which, in the limit of high number of reflectors, leads to the description of the conventional Fabry-Pérot resonator. The case studied in this article with the unequal spacing of scatterers is clearly challenged by this ideal case. The phases of the light scattered by the individual ions are less and less likely to add up perfectly constructively for increased number of emitters and for the small range of scanned U_{tip} . On the other hand, in the range of particle numbers corresponding to our measured case of several tens, the points of significantly high constructive interference should be still found within the practical limits of the ion trapping apparatus.

We have analysed the scaling of the observed maximal interference peak width observed within the voltage range where ion crystal remained stable in our trapping and cooling conditions, as presented in the main text. The analysis has been realized on the simulated interference patterns fitted to best match the observed data. As expected, multi-emitter interference narrows the width of the maximum interference peaks, similarly as for symmetrical multi-beam interference case. As can be seen in the Fig. S3, estimated observable maximum peak width corresponding to the change of the phase delay $\delta\varphi$ has been clearly steadily decreasing for all measurements up to 10 ions. This dependence seem to saturate, as the full width at half maximum (FWHM) of the observed highest interference peak for 10 and 20 ions are $0.18\ \mu\text{m}$ and $0.17\ \mu\text{m}$, respectively. This occurs because the measurements and analysis is restricted to the voltages employed in our experiment, with U_{tip} varying from 5 V to 900 V, which for ion numbers beyond 4 doesn't cover the full period of the interference pattern. The presented graph nevertheless demonstrates a steady increase in the spatial phase resolution in the measured ion number range which points on the increase of the coherently contributing number of scatterers. We note that we exclude the measurements from more than 20 ions in this consideration, because their interference patterns were influenced

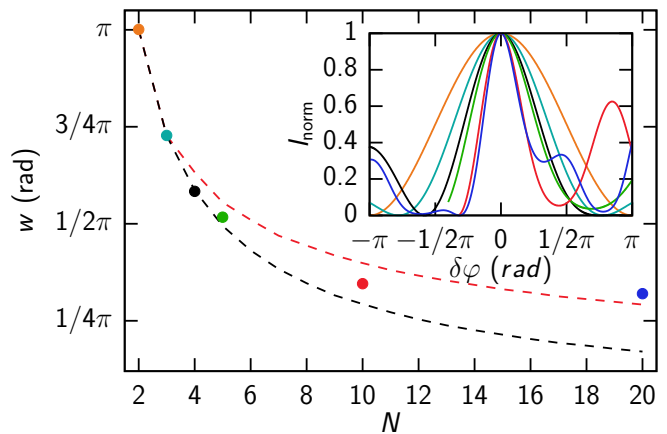


FIG. S3. The analysis of the phase interference pattern phase sensitivity in the simulated fringes. The figure shows the full width at half maximum widths (FWHM) w of observed maximal interference peaks for the measured strings containing N ions. The widths are evaluated from the simulations fitting the experimental data and the corresponding interference peaks with their heights normalized to the unit value are shown in the inset. The spatial dimension on the horizontal axis has been normalized to the obtained distance between two ions for a given voltage U_{tip} , which unifies the length scale for the realized measurements with different ion numbers and different measured axial voltage ranges. The dashed black and red lines correspond to the widths of maximum intensity peaks in the interference patterns for the equidistant strings with the distance scaled to the smallest and largest distance between neighbouring ions in the harmonic case. The inset shows the simulated interference maxima from which the widths were estimated. The colours of the data points in the main graph are set to match the colours of the corresponding interference peak shown in the inset.

by the limited spatial extent of the exciting 397 nm laser beam, which effectively causes broadening of its structure and it is therefore not relevant for the presented analysis.

We have further analysed the scaling of the observed maximal interference peak intensity within the voltage range measured in our experiment. We have evaluated the maximum intensity after normalizing the light scattered by each ion to one. The observed dependence growth is expected to be naturally limited by the finite probability of the coherent scattering process and by the non-equidistant spacing between the neighbouring scatterers. The Fig. S4 shows the measured normalized peak intensities plotted as a function of the ion number N in our setup (green diamonds). The red dashed line shows the estimated case with fully incoherent scattering for the same ion numbers corresponding to the incoherent sum of scattered unity intensities. Importantly, the presented measured data show the intensity substantially higher than this incoherent case for all analysed cases up to 20 ions. Note the square root vertical axis scaling used for improving the readability. The upper bound of the scaling for emitters in harmonic trap would corre-

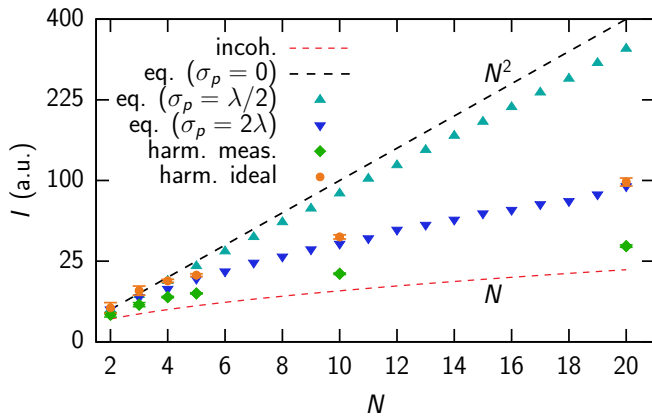


FIG. S4. Analysis of the maximal observable scattered light intensity in the measured interference patterns. The two limiting cases of fully incoherent scatterers and fully coherent equidistant scatterers mark the relevant intensity scale shown as red and black dashed line, respectively. All the data are normalized to unit intensity per scatterer. Note the square scaling of the vertical graph axis. The normalized measured maximal intensities of light scattered by emitters in the harmonic potential (green diamonds) are always substantially surpassing the fully incoherent case. If the scattering would be considered fully coherent, the measured data would be approaching the limit (orange circles) given by the subtraction of the incoherent background. For comparison with the equidistant case, we show the case of fully coherent scattering by quasi-equidistant scatterers with a Gaussian distribution of individual positions around the ideal equidistant case (blue triangles). *Eq.* and *harm.* denote the equal and harmonic spacing case, respectively, and σ_p is the variance in the positions of ions.

spond to fully coherent scattering observable within the measured tip voltage ranges marked by orange circles. These are evaluated from the simulated ideal interference patterns by looking for the observable intensity maxima. As expected, the maximum intensities seem to be much lower than in the case corresponding to the fully coherent and perfectly equally spaced emitters (black dashed line). On the other hand, from experimental point of view relevant for further applicability of the presented

results, it is worth noting that the idealized distribution of the perfectly equidistant scatterers is extremely hard or even impossible to achieve in most physical platforms. That is due the high sensitivity to even small asymmetry of the mutual distance between emitters or unbalance of their intensities. To allow for some rough comparison of realistic cases we have included the simulation of scattering from particles which have some random but fixed Gaussian uncertainty σ_p in their position around the idealized center position corresponding to the equidistant case. The presented simulations correspond to the average from 100 random realizations. While few experimental platforms could with enormous effort reach the sub-wavelength deterministic equidistant positioning of single emitters and, at the same time, their sub-wavelength spatial extent, most of these realizations will be actually limited to the precision on the order of scattered light wavelength which will give a limit on the precision of detection of the particle position. The simulations corresponding to $\sigma_p = \lambda/2$ and $\sigma_p = 2\lambda$ are shown by light blue and dark blue triangles, respectively. These results show that the position error of $\sigma_p = 2\lambda$ would be almost equivalent to the presented non-equidistant case corresponding to harmonic potential within the considered number of scatterers. It is important to recall here that the presented non-equidistant case formed by the quadratic potential and the mutual Coulomb repulsion defines the relative position of the scatterers in a predictable fashion and with very small uncertainty. This is contrary to the equidistant case where scatterers have to be typically positioned independently by creation of many individual binding potentials. A promising alternative to these cases is represented by trapping of scatterers in optical lattices or configurable arrays of optical tweezers, where trapping potentials formed at multiples of trapping light wavelength can be naturally equidistant and their distance can be tuned in principle independently with respect to the wavelength of the scattered light. These systems could present a viable alternative for application of the presented results, provided that the spatial localization of employed scatterers in individual trapping sites is suppressed to a small fractions of the scattered light wavelength [S4, S5].

[S1] D. F. V. James, *Appl. Phys. B* **66**, 181 (1998).
[S2] A. Härter, A. Krüchow, A. Brunner, and J. H. Denschlag, *Appl. Phys. B* **114**, 275 (2014).
[S3] M. Brownnutt, M. Kumph, P. Rabl, and R. Blatt, *Rev. of Mod. Phys.* **87**, 1419 (2015).
[S4] D. Barredo, S. De Léséleuc, V. Lienhard, T. Lahaye, and

A. Browaeys, *Science* **354**, 1021 (2016).
[S5] H. Bernien, S. Schwartz, A. Keesling, H. Levine, A. Omran, H. Pichler, S. Choi, A. S. Zibrov, M. Endres, M. Greiner, V. Vuletić, and M. D. Lukin, *Nature* **551**, 579 (2017).